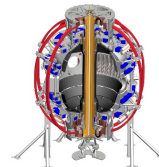
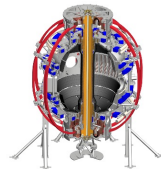


The high-Z challenge and advances in core x-ray spectroscopy

Luis F. Delgado-Aparicio (PPPL), Advanced Projects Department

Princeton, PPPL, 06/21/2024

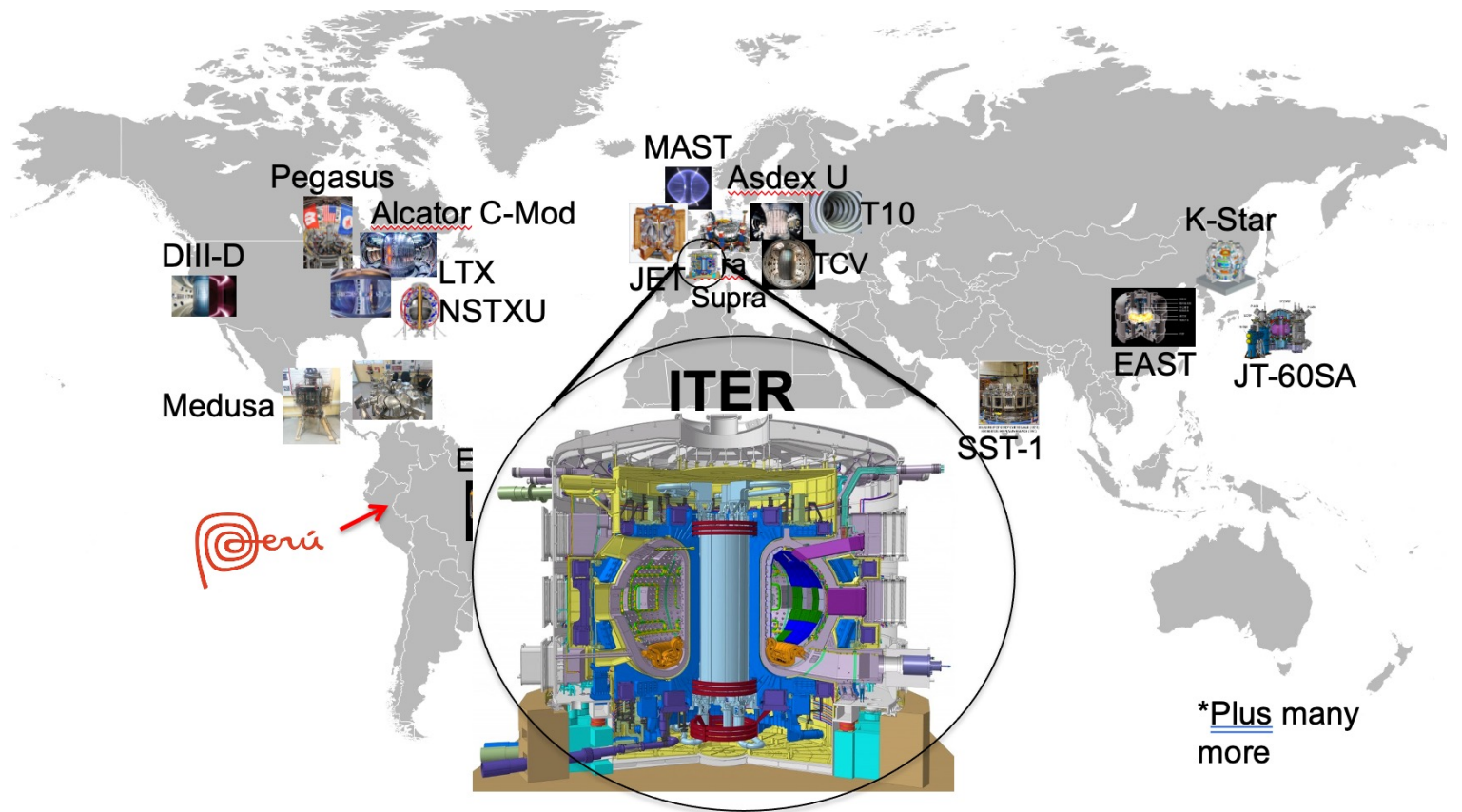




Outline

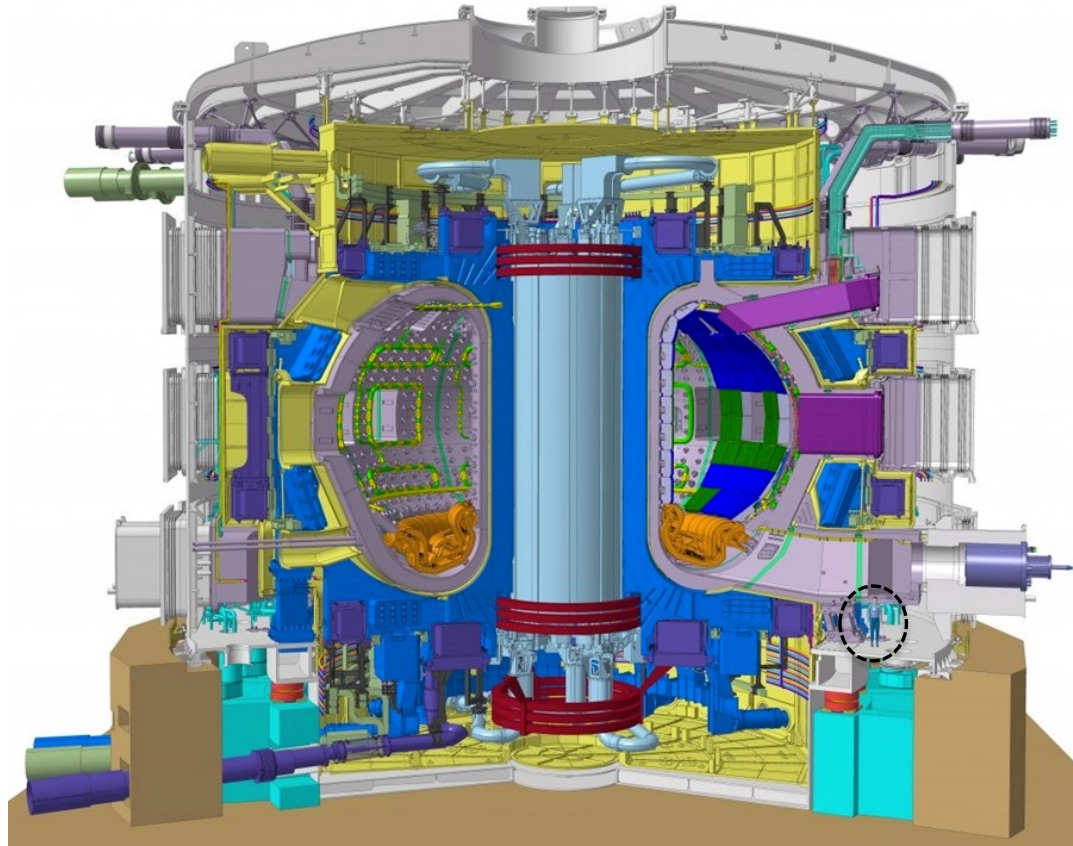
- ① Magnetically confined fusion (MCF) plasmas and the Z-challenge
- ② Radiation and the basic need of x-ray spectroscopy?
- ③ Take home message: three types of x-ray diagnostics
- ④ Summary

Tokamaks (and stellarators) spread around the world study different plasma parameters and shapes



ITER will be the first time we have net energy (more energy OUT than IN)

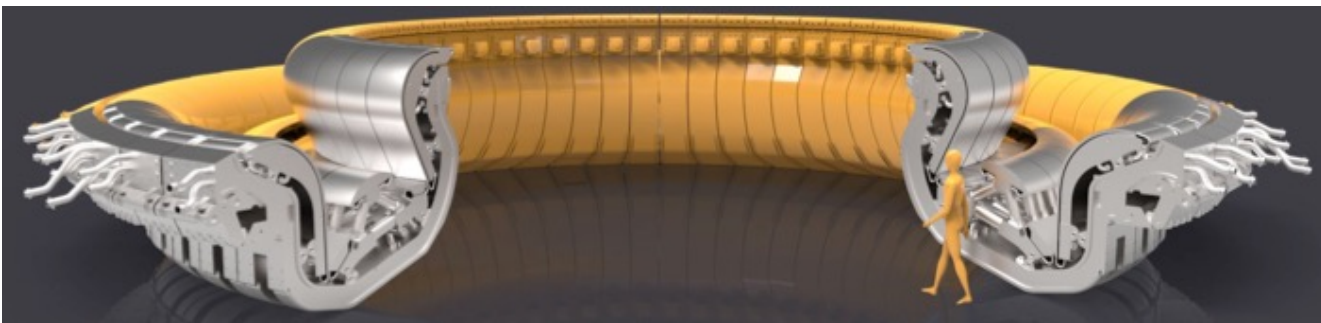
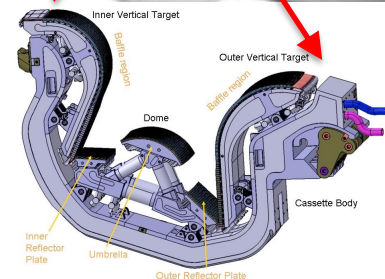
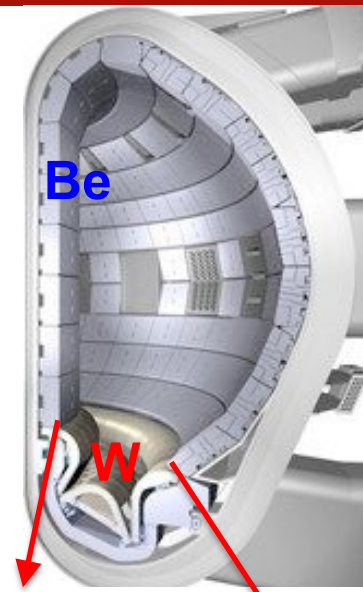
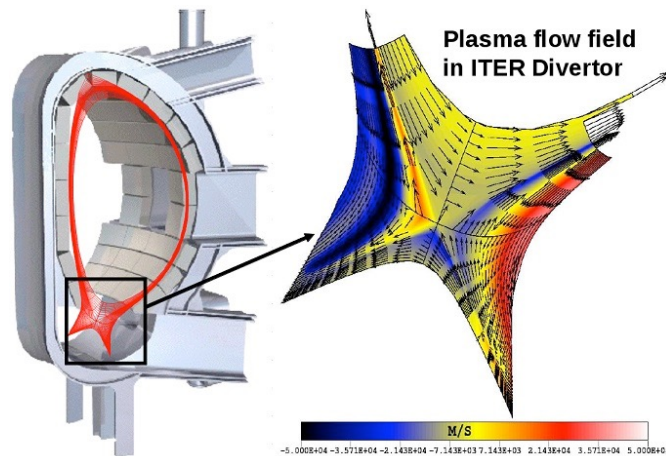
- ITER is a collaboration between USA, EU, China, Japan, Korea, India and Russia
- It's expected to produce 500MW of power using 50MW to run ...this is the 1st time in history where $P_{out} > P_{in}$
- First plasmas “expected” by 2025
 - Many challenges ahead!
 - The Z-challenge?
(low-Z vs high-Z)



With the help of detailed simulations ITER scientists “decided” on a wall covered with low- and high-Z PFCs

Simulations of plasma flows and plasma-wall interaction have had a decisive influence on the design of ITER wall

⇒ It's a decision on the edge conditions which will alter core performance

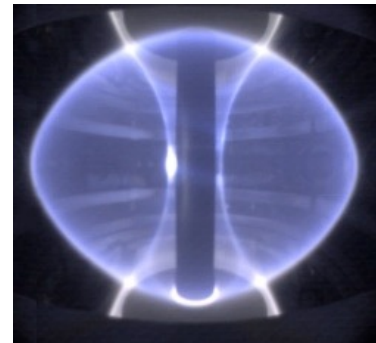


Edge localized modes (ELMs) and disruptions can impact integrity of divertor cassettes

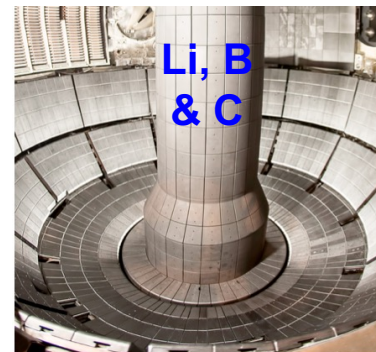
The low-Z (Li, Be, C, B) vs high-Z (Fe, Mo, W) plasma facing component (PFC) challenge - **IDEAL**

Both low- & high-Z materials are currently being used for the **PFCs**, but each has technological hurdles.

MAST, CCFE,
Oxfordshire, UK



NSTX-U @ PPPL,
Princeton, NJ



① Low-Z materials:

- a) Typically have **higher erosion rates**
- b) Their injection into the main chamber will result in an **increase of Z_{eff}** and **collisionality** ($\nu_{e,Z}$).
- c) H-, D- & **T-retention** is a difficult issue!

② Augment of Z_{eff} will lead to:

- a) **Reduce fuel purity** (n_D/n_e) and **reactivity** ($S_n \propto n_D^2$ or $n_D n_T$).
- b) But contributing less to radiated power density:

$$P_{\text{rad}} = n_e n_D L_D + n_e n_C L_C + \cancel{\Sigma n_e n_Z L_Z}$$

The low-Z (Li, Be, C, B) vs high-Z (Fe, Mo, W) plasma facing component (PFC) challenge - REAL

③ Conversely, high-Z materials have good properties as a PFCs:

- Low H/D/T retention.
- High-heat tolerance (e.g. high melting points)
- Low erosion (sputtering) rates.
- Small contribution to Z_{eff} :

$$Z_{\text{eff}} = n_D/n_e + 36n_C/n_e + \sum (n_Z/n_e) Z^2$$

④ However, if high-Z impurities accumulate to any substantial level (e.g. high- n_Z/n_e), this will lead to:

a) Exponentially enhance the **radiation power losses** ($\propto Z^4$): $P_{\text{rad}} = n_e n_D L_D + n_e n_C L_C + \sum n_e n_Z L_Z$

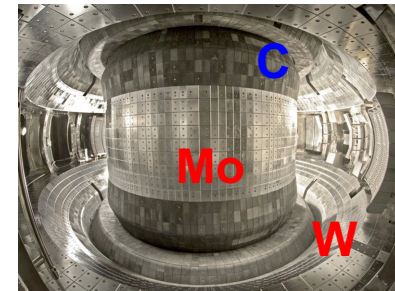
b) **Reduce the heating efficiency** and modifying the overall **power balance**

c) **Radiation collapse**

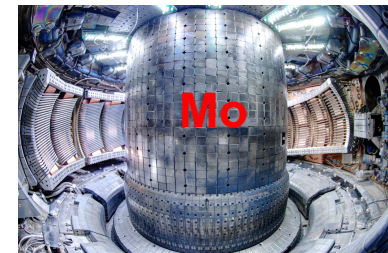
Tore Supra/WEST in France



EAST in China



C-Mod @ MIT, USA



The low-Z (Li, Be, C, B) vs high-Z (Fe, Mo, W) plasma facing component (PFC) challenge - REAL

③ Conversely, high-Z materials have good properties as a PFCs:

- a) Low H/D/T retention.
- b) High-heat tolerance (e.g. high melting points)
- c) Low erosion (sputtering) rates.
- d) Small contribution to Z_{eff} :

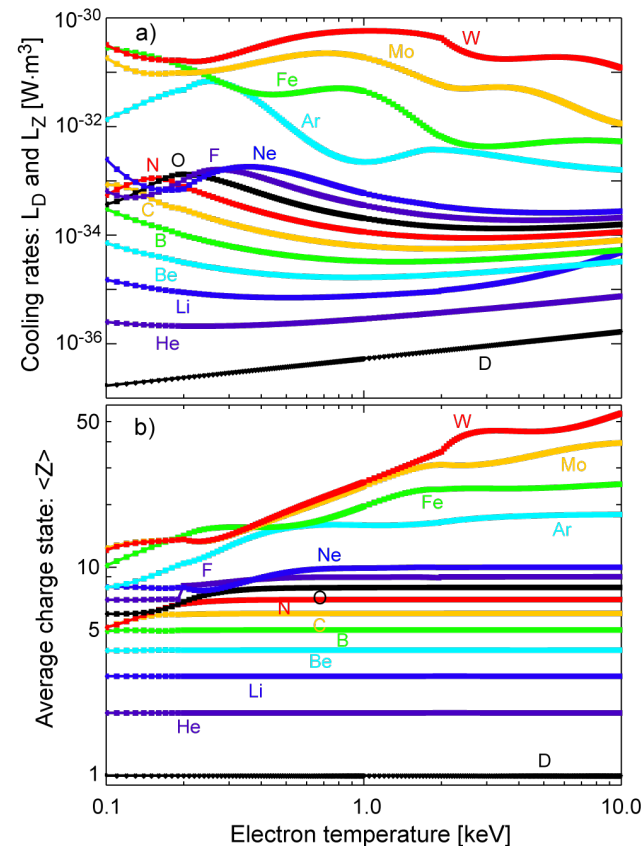
$$Z_{\text{eff}} = n_D/n_e + 36n_C/n_e + \sum (n_Z/n_e) Z^2$$

④ However, if high-Z impurities accumulate to any substantial level (e.g. high- n_Z/n_e), this will lead to:

a) Exponentially enhance the **radiation power losses** ($\propto Z^4$): $P_{\text{rad}} = n_e n_D L_D + n_e n_C L_C + \sum n_e n_Z L_Z$

b) **Reduce the heating efficiency** and modifying the overall **power balance**

c) **Radiation collapse**



Radiative power densities (vis/UV/x-ray) & charge state $\langle Z \rangle$ can be obtained using coronal equilibrium

Parameterizing equations of interest for two-impurity plasma

Quasi-neutrality:
$$1 = \frac{n_D}{n_e} + \langle Z_1 \rangle \frac{n_{Z1}}{n_e} + \langle Z_2 \rangle \frac{n_{Z2}}{n_e}$$

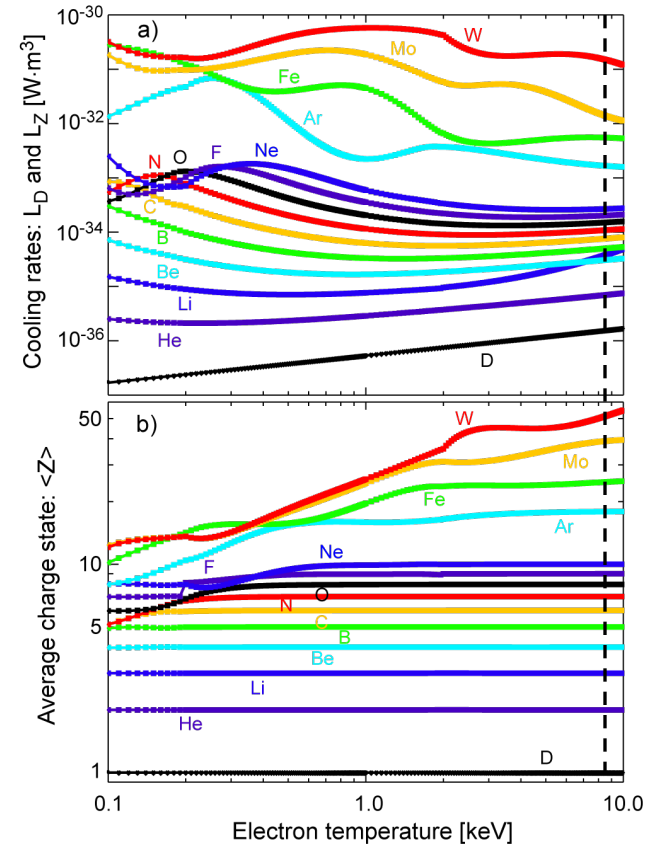
Effective charge:
$$Z_{eff} = \frac{n_D}{n_e} + \langle Z_1 \rangle^2 \frac{n_{Z1}}{n_e} + \langle Z_2 \rangle^2 \frac{n_{Z2}}{n_e}$$

Normalized radiated power density:

$$\hat{P}_{rad}^V \equiv \frac{P_{rad}^V}{n_e^2 L_D} = \frac{n_D}{n_e} + \frac{n_{Z1}}{n_e} \frac{L_{Z1}}{L_D} + \frac{n_{Z2}}{n_e} \frac{L_{Z2}}{L_D}$$

Hydrogenic cooling rate:

$$L_D = 5.35 \times 10^{-37} T_e^{1/2} [\text{keV}] \text{ W} \cdot \text{m}^3$$



Why is important to measure x-rays emitted from tokamak and stellarator fusion-grade plasmas ?

- ① A significant fraction of the power delivered to the plasma is lost in the form of radiation [even in an ideal pure H plasma].
- ② A subset of P_{rad} : In real conditions could be as high as 90%.
- ③ X-rays are the most dominant source of radiation from hot plasmas: $h\nu \sim T_e$:
Exercise: For $100 \text{ eV} < T_e < 20 \text{ keV} \Rightarrow 0.5 < \lambda < 130 \text{ \AA} \Rightarrow \text{X-rays!}$
- ④ Measurement of power losses in the x-ray range enable the characterization of parameters such as, n_e , n_Z , T_e , T_i , v_ϕ , v_θ , to be used in describing/studying:
 - a) MHD and reconnection events (from hot core to cold edge).
 - b) Transport coefficients (e.g. diffusivity and pinch velocity).
 - c) Radial electric field (E_r)
 - d) Magnetic flux-surface reconstructions: $T_e(\psi) \Rightarrow J$ and q

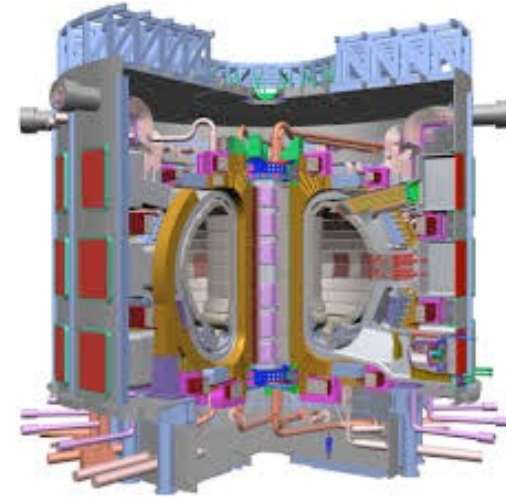
THE X-RAY CASE: ...how to diagnose x-rays from thermonuclear plasmas ?



X-Ray Goggles



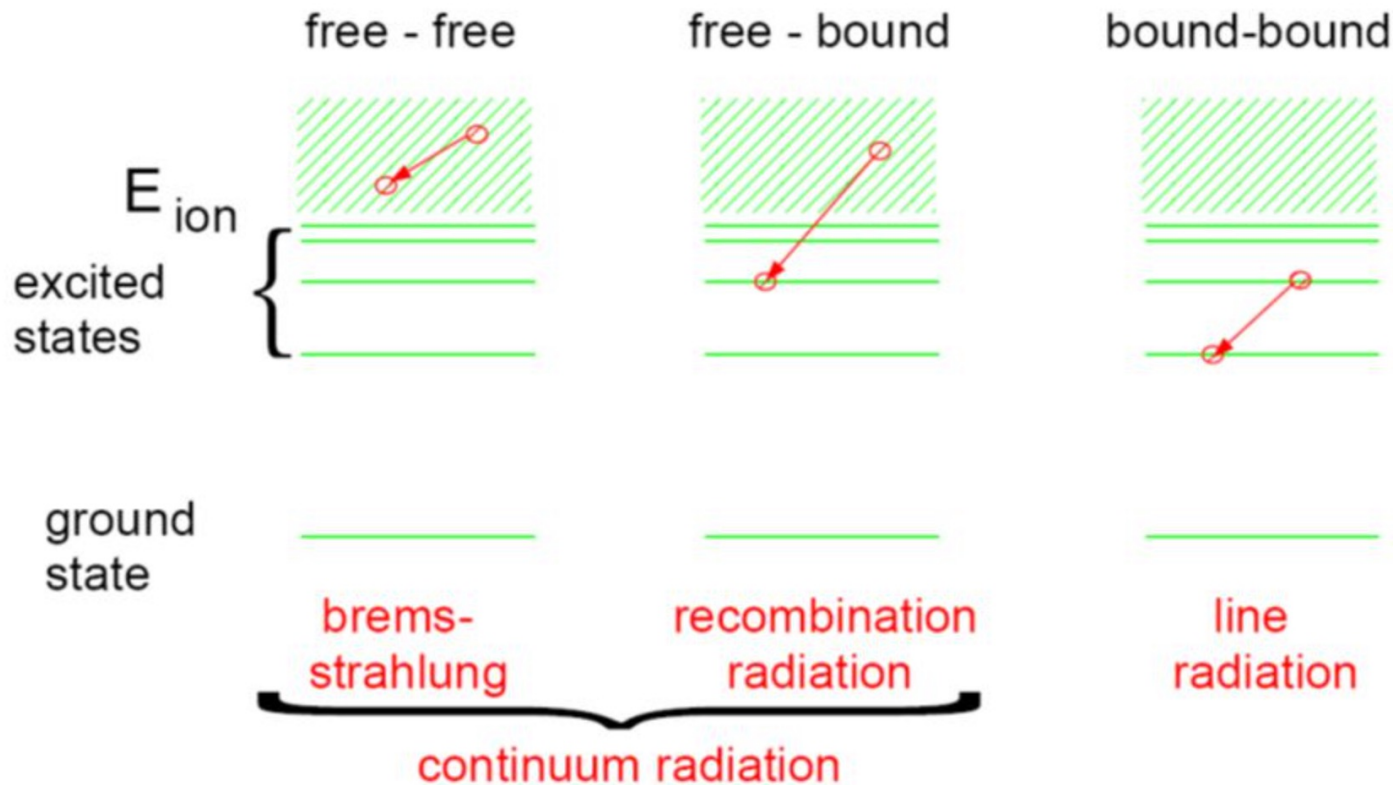
Nearly 90% of the radiated power in ITER will be in the x-ray range ($V_{\text{ITER}} \sim 840 \text{ m}^3$)



SXR: $1 < E < 20 \text{ keV}$

HXR: $20 < E < 400 \text{ keV}$

Main radiation mechanisms: Bremsstrahlung (ff), radiative recombination (fb) & line-emission (bb)



Coronal equilibrium (ionization charge balance)

- Commonly used in fusion plasmas and in the solar corona
- Assumes three body-recombination rate is small
- Balance between electron-impact ionization & radiative recombination

$$\underbrace{n_e n_Z \mathcal{S}_{Z \rightarrow (Z+1)}(T_e)}_{\text{Ionization}} = \underbrace{n_e n_{(Z+1)} \alpha_{Z+1 \rightarrow Z}(T_e)}_{\text{Recombination}}$$

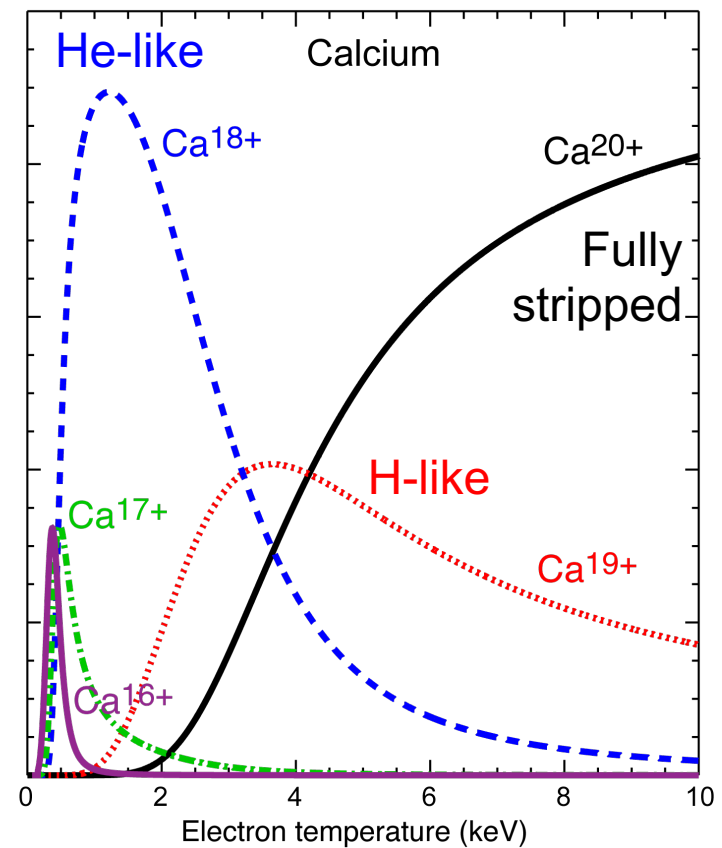
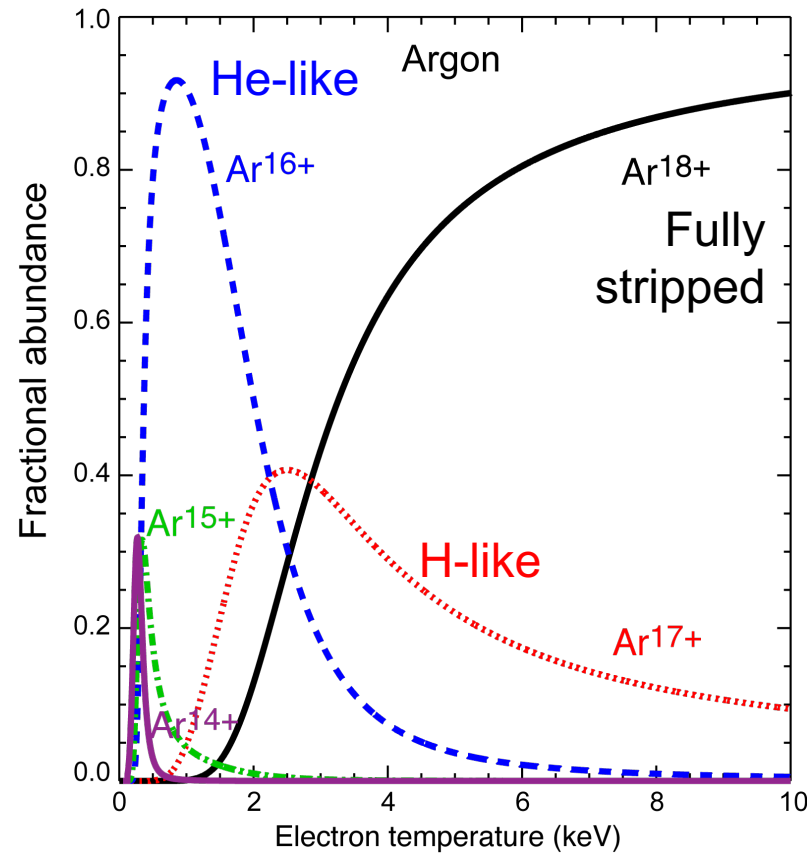
$$\Rightarrow \frac{n_{(Z+1)}}{n_Z} = \frac{\mathcal{S}_{Z \rightarrow (Z+1)}(T_e)}{\alpha_{Z+1 \rightarrow Z}(T_e)}$$

- Result: Ionization degree is independent of density and increases with T_e
 - Low-Z ions (Be, B, C) are often fully stripped

Fractional abundance calculations (n_{ij}/n_i) depend only on the local electron temperature (issues with nomenclatures ???)

Argon
Z=18
A~40
18 protons
22 neutrons

Calcium
Z=20
A~40
20 protons
20 neutrons

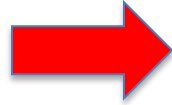


Local emission has to be calculated on plasma parameters $[T_e, n_e, n_Z(R,t)]$

1. Continuum and & line emission:

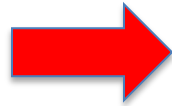
Bremsstrahlung (ff):

$$\frac{d\mathcal{P}_{ff}^{ij}(T_e, E)}{dE} \propto \frac{n_e^2 C_i(n_{ij}/n_i) Z_{ij}^2}{T_e^{1/2}} \mathcal{G}_{ff}(Z, T_e, E) \exp(-E/T_e)$$



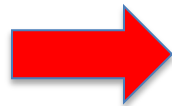
Radiative recombination (fb):

$$\frac{d\mathcal{P}_{fb}^{ij}(T_e, E)}{dE} \propto \frac{n_e^2 C_i(n_{ij}/n_i) Z_{ij}^2}{T_e^{1/2}} \beta_{ij}(T_e, E) \exp(-E/T_e)$$

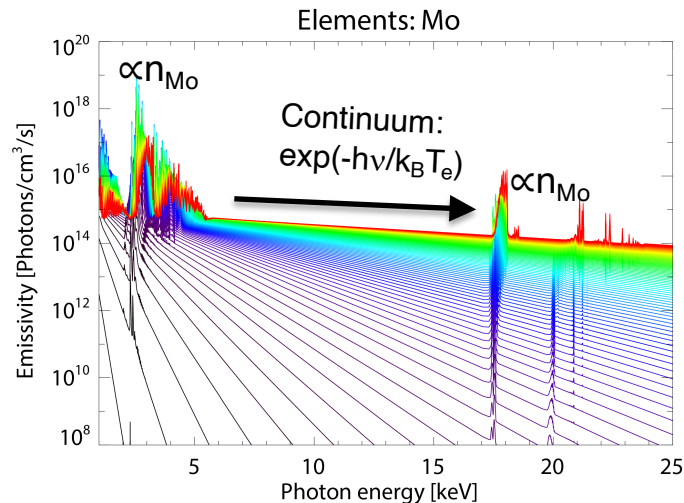
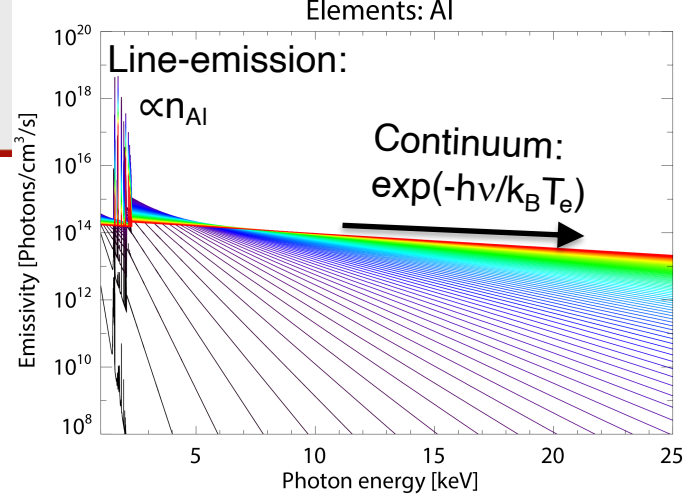


Line emission (bb):

$$\frac{\mathcal{P}_L^{ij}(T_e, E)}{E_L} \propto n_e^2 C_i(n_{ij}/n_i) \langle \sigma v(T_e, E)_{ij} \rangle$$



0.1 T_e [keV] 10



SXR brightness measurements are line-integrated along detection sightlines

2. Visible/UV/x-ray tomography:

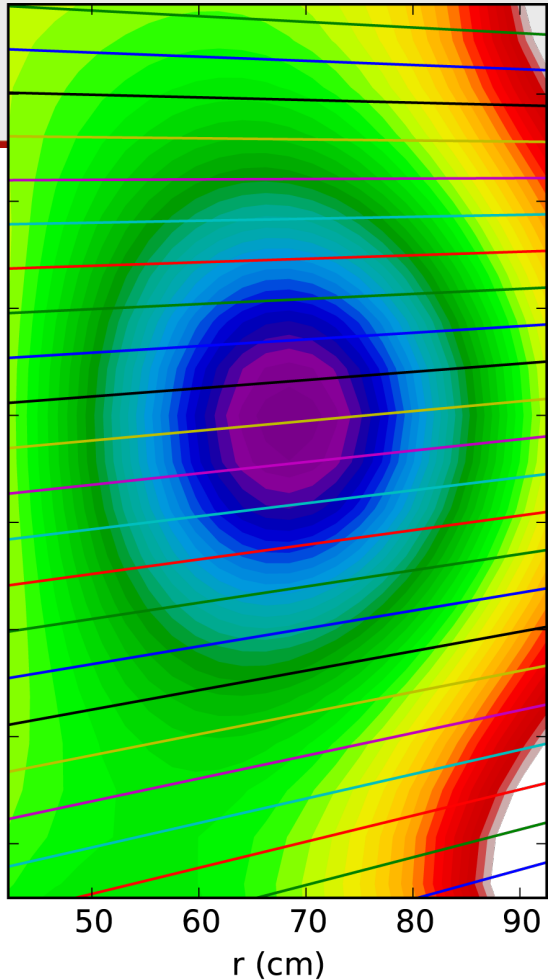
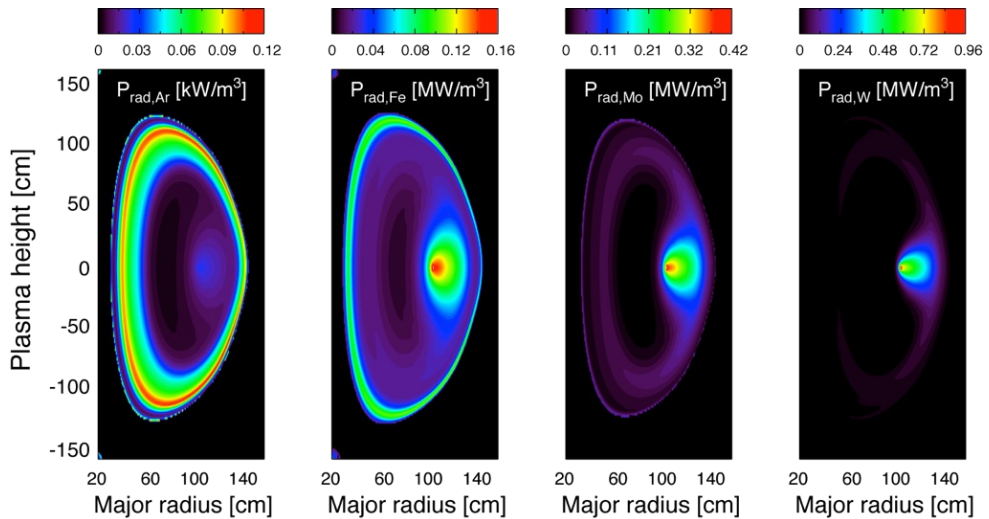
- Emmissivity is a flux-surface function
- Inversion ($B=M \times E \Rightarrow E=M^{-1} \times B$)



3. Transport/heating asymmetries (warning):

Example:

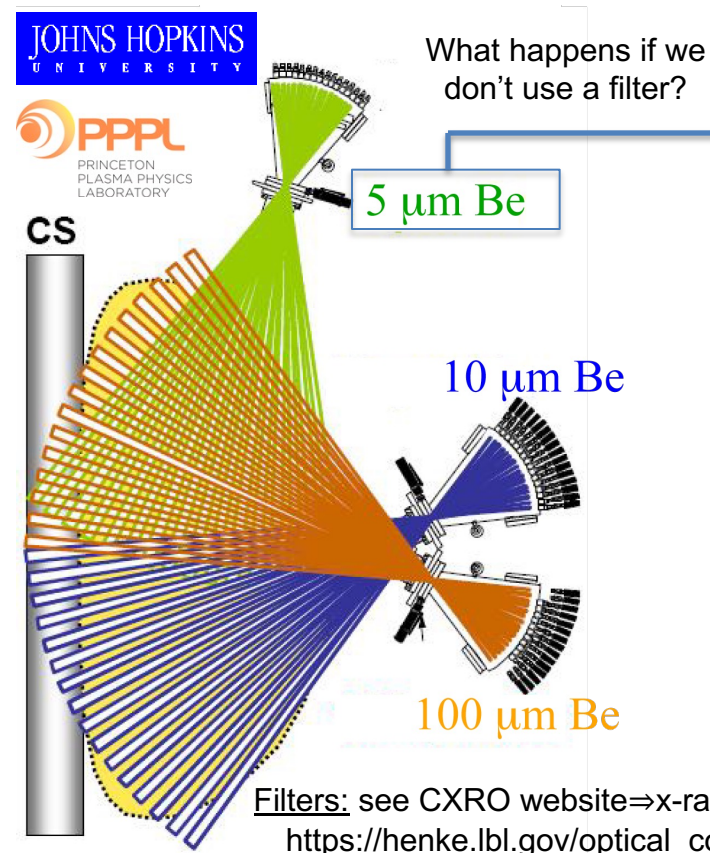
Core radiation from medium- to high-Z will be affected by centrifugal forces



Take home message: You have three alternatives (...but with multiple detection options) in the x-ray range !

- ① **Conventional broadband x-ray measurements**
(e.g. SXR tomography \Rightarrow confinement, MHD, equilibrium)
- ② **Doppler line-radiation x-ray measurements**
(e.g. n_Z , T_e , T_i , v_ϕ , v_θ , \Rightarrow calculation of E_r)
- ③ **Modern broadband PHA & multi-energy measurements**
(e.g. Z_{eff} , n_Z , T_e , $n_{e,\text{fast}}$)

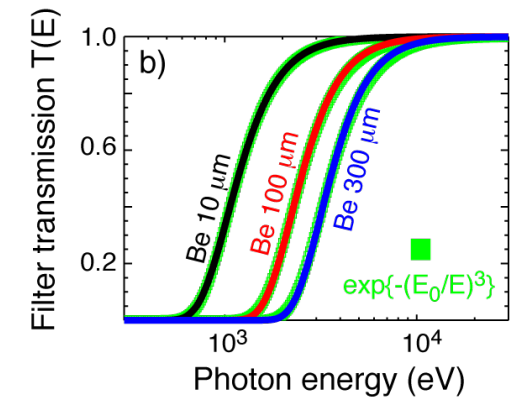
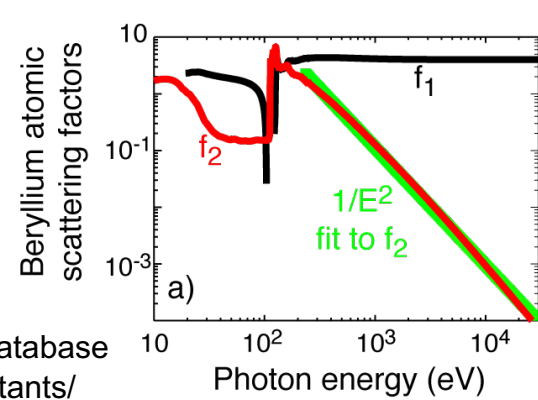
1.- Conventional SXR tomography consists of an array of diodes/detectors integrating the local plasma emissivity



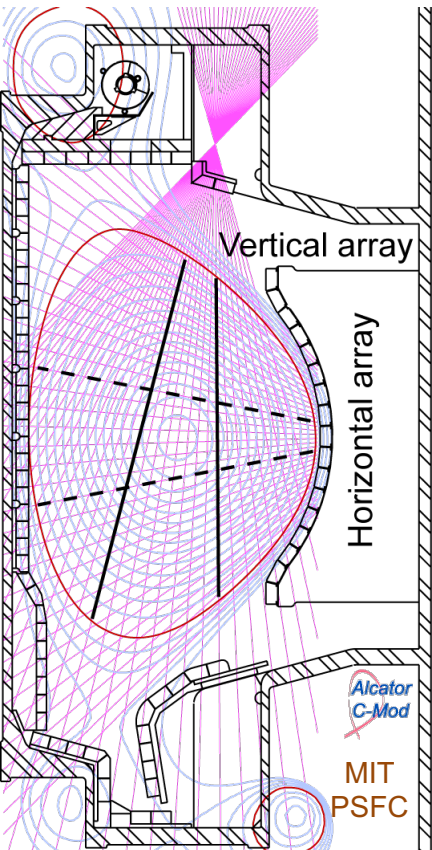
① Essential elements:

- Pinhole (radial resolution vs integration)
- Thin vs thick metallic filters
- Current mode: SXR Si-based diode or diode-array
- Current mode: X-ray scintillator + FoP + FO + PMT
- Transimpedance amplifier (10^4 - 10^7 V/A) + DAQ

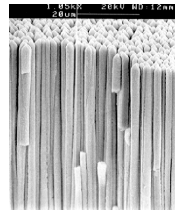
② Metal filters discriminate edge/core effects (peeling the "onion")



Conventional SXR tomography integrates in photon-energy using metal filters diode arrays and TIAs

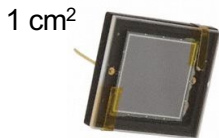


Indirect detection with scintillator (e.g. CsTI - green)

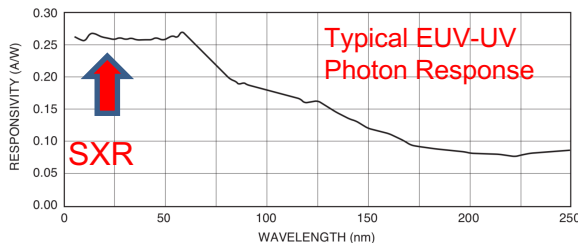
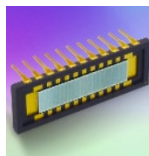


Direct x-ray detection (e.g. Si diodes)

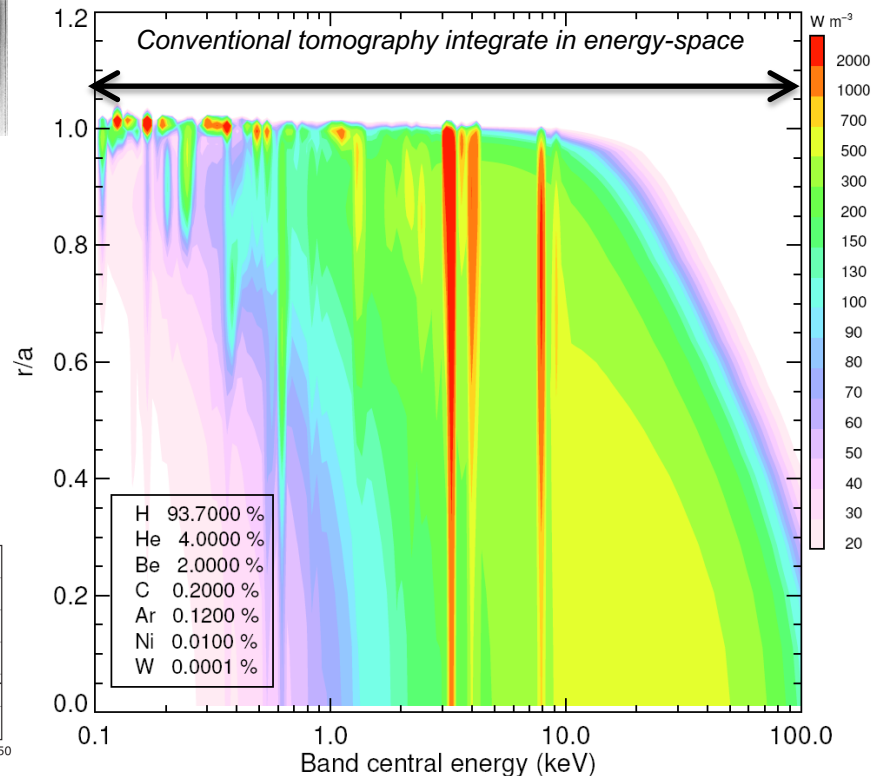
AXUV-100



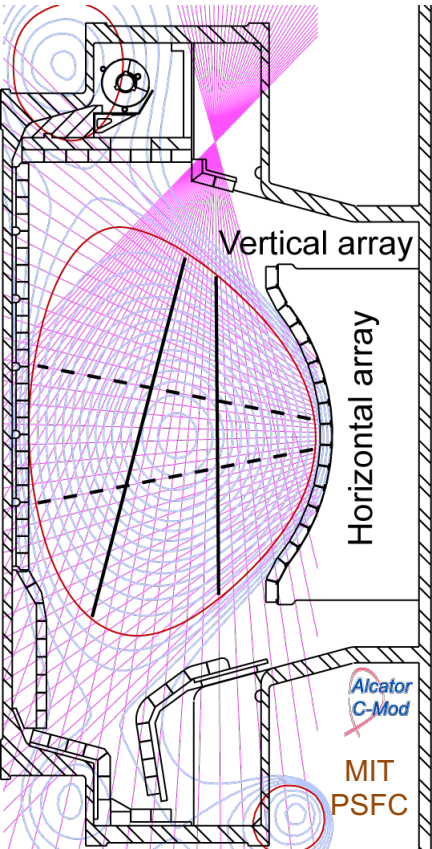
AXUV-20



Example of spatially resolved x-ray spectra from ITER



Spatial and energy integration means also that it is very difficult to extract local plasma parameters from emission



SXR systems measure line-integrated continuum & line-emission

n_e : electron density; n_i : ion (H, D/T) density

n_Z : impurity density (He, B, C, O, Ar, Mo, W)

T_e : electron temperature; “Maxwellian” distributions $f(E_e/k_B T_e)$

θ -asymmetries as $F[v_\phi$: toroidal velocity, M_Z : ion mass]
(vertical or tangential views are needed)

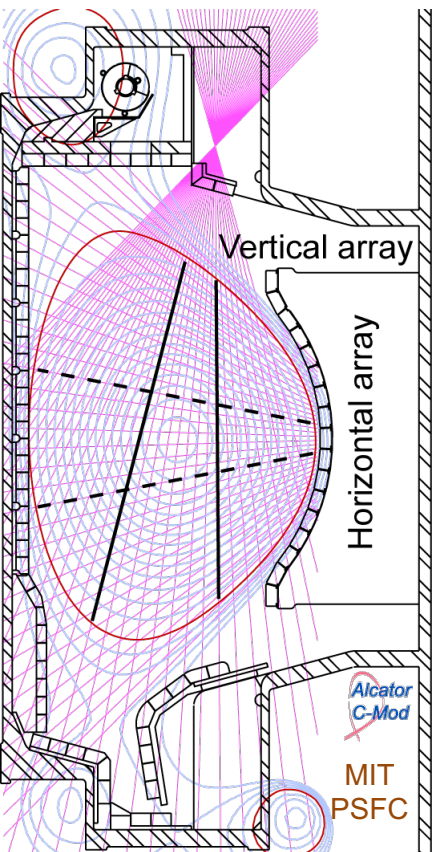
L : Length of integration, θ : poloidal angle
(radial and poloidal coverage)

Energy
response

$T_{\text{filter}}(E_{\text{ph}})$: transmission function of filter

Detector response: $S(E_{\text{ph}})$

However, conventional SXR tomography is still being used for stability, MHD & transport studies

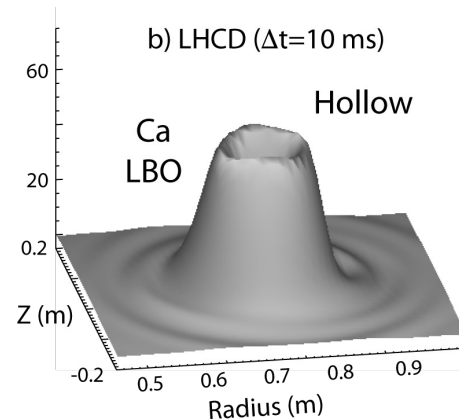
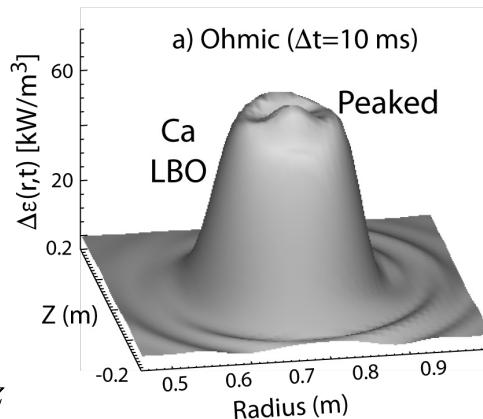
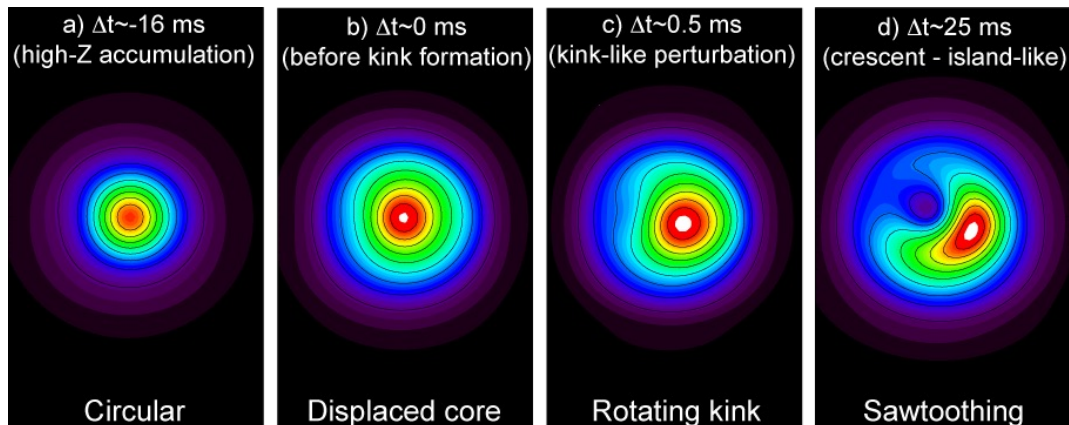


a) Stability and MHD [e.g. (m,n) modes and sawteeth]

b) Impurity transport (e.g. using gas injection or LBO)



$$\Gamma_Z = -D_Z \nabla n_Z + V_Z n_Z$$



Take home message: You have three alternatives (...but with multiple detection options) in the x-ray range !

① **Conventional broadband x-ray measurements**
(e.g. SXR tomography \Rightarrow confinement, MHD, equilibrium)

② **Doppler line-radiation x-ray measurements**
(e.g. n_Z , T_e , T_i , v_ϕ , v_θ , \Rightarrow calculation of E_r)

③ **Modern broadband PHA & multi-energy measurements**
(e.g. Z_{eff} , n_Z , T_e , $n_{e,\text{fast}}$)

We also need to extract local plasma information !!!

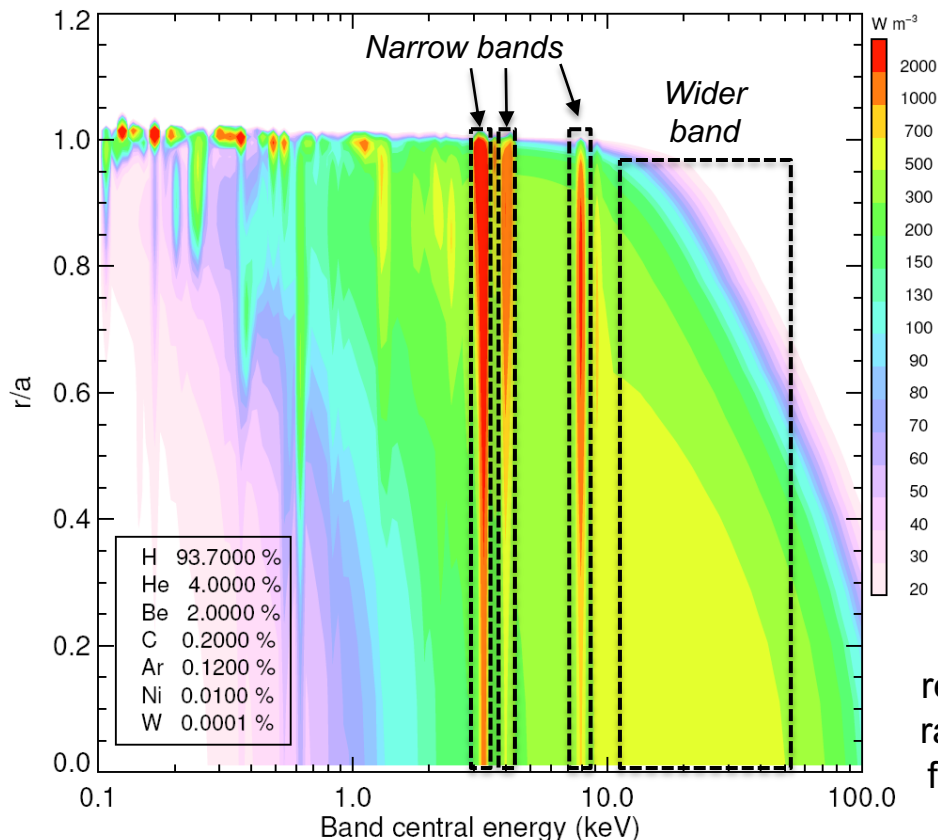
How to extract plasma physics parameters from narrow and/or wider SXR and HXE energy bands ?

Narrow energy bands

- Doppler spectroscopy
- High-resolution spectrometers
 - $E/\Delta E \sim 5000-200000$
- Probes mainly the ion-channel
 - $T_i, V_{\phi,\theta}, n_Z \dots T_e$ (line-ratios)

Wider energy bands

- Multi-energy spectroscopy
- Low-resolution spectrometers
 - $E/\Delta E \sim 10-50$
- Probes e^- and ion channels
 - $T_e, n_Z, \Delta Z_{\text{eff}}, Z_{\text{eff}}$
- $n_{e,\text{fast}}$ (e.g. LHCD, runaways)



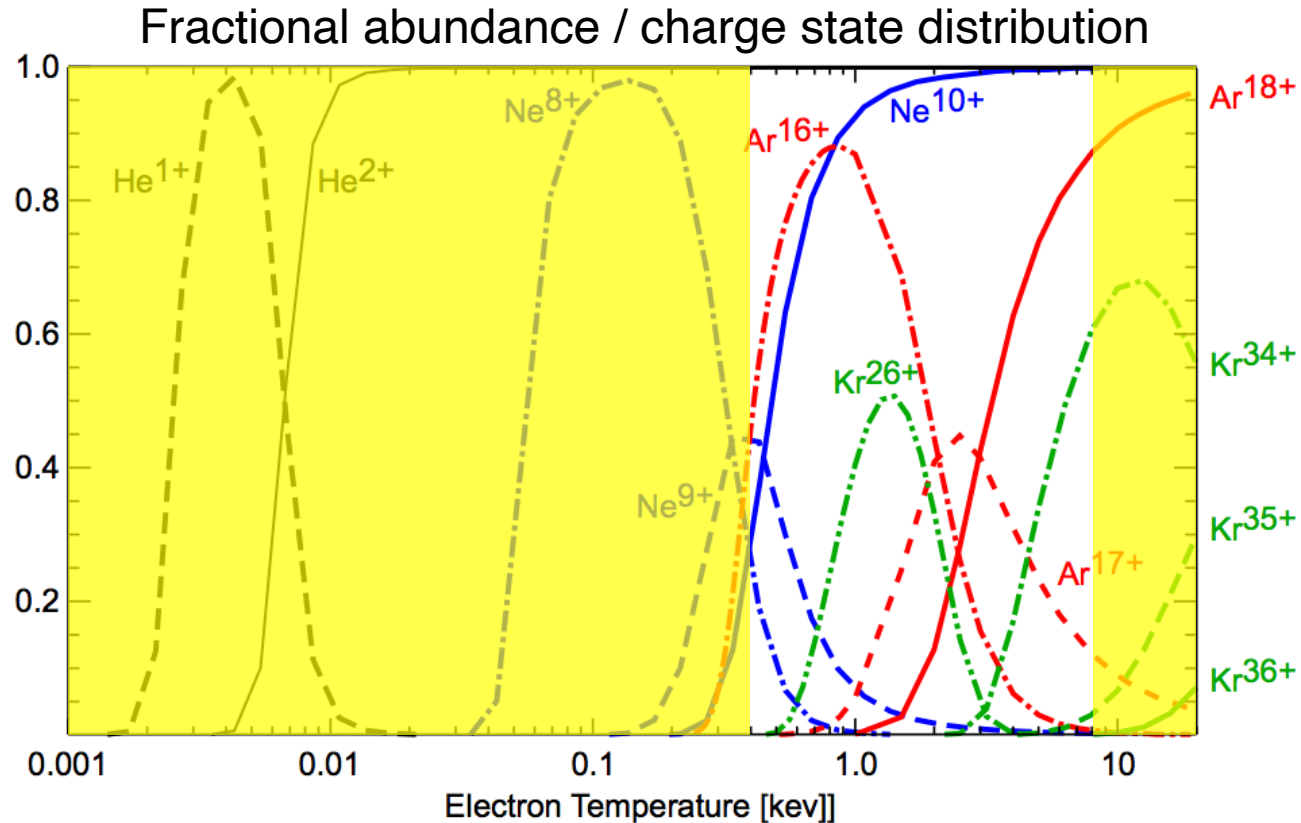
Spatially resolved x-ray spectra from ITER

X-ray crystal imaging spectrometers enable $T_{i,e}$, $v_{\phi,\theta}$ and n_Z 's measurements via Doppler broadening & line shifts.

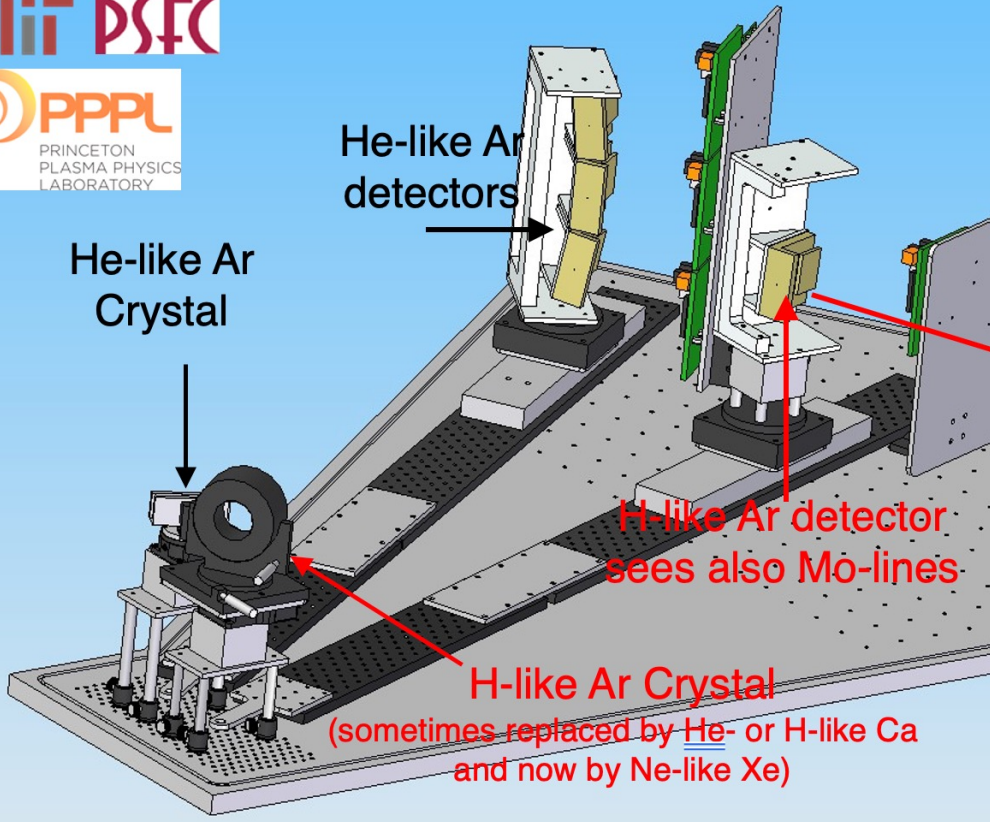
- ① Not all reactor concepts consider NBI's (CXRS). Spontaneous rotation ($\propto W_{\text{MHD}}$) may provide the solution for stabilization.
- ② Measurement of ion-temperature (T_i), toroidal and poloidal velocity ($v_{\phi,\theta}$) and impurity density (n_Z 's) are important for understanding and optimizing confinement:
 - a) ∇T_i driven turbulence (ITG) is a leading candidate for explaining anomalous ion thermal transport.
 - b) V_ϕ and dV_ϕ/dr play important roles in the H-mode transition, ITB-formation, and RWM-stabilization.
 - c) Radial electric field ($\propto n_Z, T_i, v_{\phi,\theta}$)
 - d) Z-transport/accumulation needs to be studied & controlled/avoided

Choosing the appropriate (non-perturbative \Rightarrow low n_z & P_{rad}) extrinsic impurity gas-puff to do x-ray spectroscopy

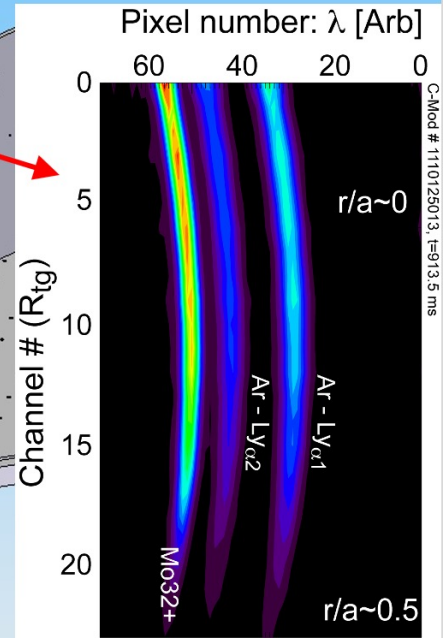
- ① For the $T_e \in [0.5, 5]$ keV, **He** & **Ne** are fully stripped except in the cool edge region.
- ② H- and He-like **Ar** are dominant $T_e \in [0.5, 5]$ keV
- ③ **Kr** or **Xe** could be used for diagnosing the core $T_e \in [4, 20]$ keV, but they are more “*perturbative*” than Ar for the same absolute density,
 \Rightarrow puff less Kr/Xe



X-ray crystal imaging spectrometers revolutionized our field with T_i and $V_{\phi,\theta}$ profile measurements



Ne-like Mo and H-like Ar fall in the spectrum



Similar systems have been installed in NSTX, KSTAR, EAST, LHD, W7 and in the future, NSTX-U, WEST, JT60SA & ITER

Focusing properties of spherical x-ray crystal

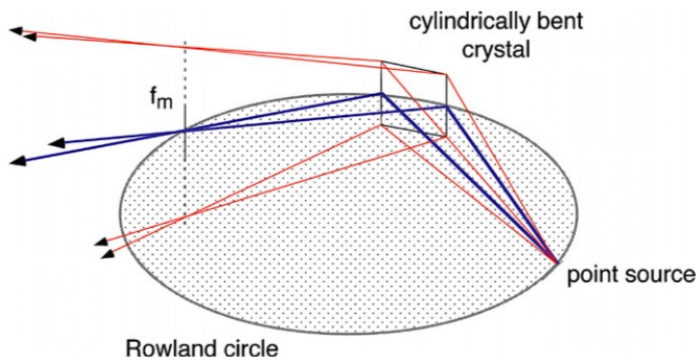


Figure 6. Focusing properties of a cylindrically bent crystal illustrating the divergence of sagittal rays.

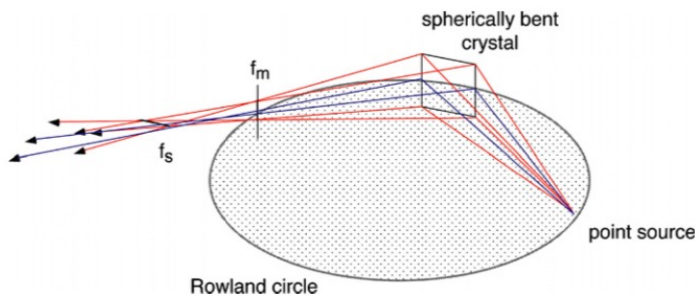
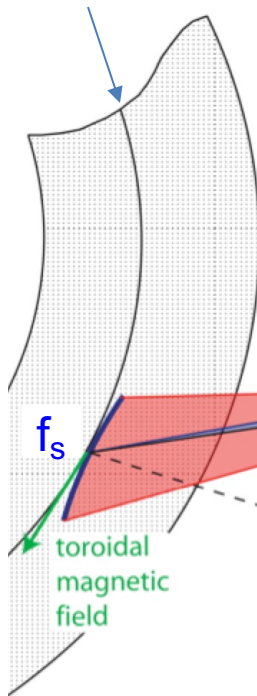


Figure 7. Focusing properties of a spherically bent crystal illustrating the focusing of sagittal rays.

Magnetic axis

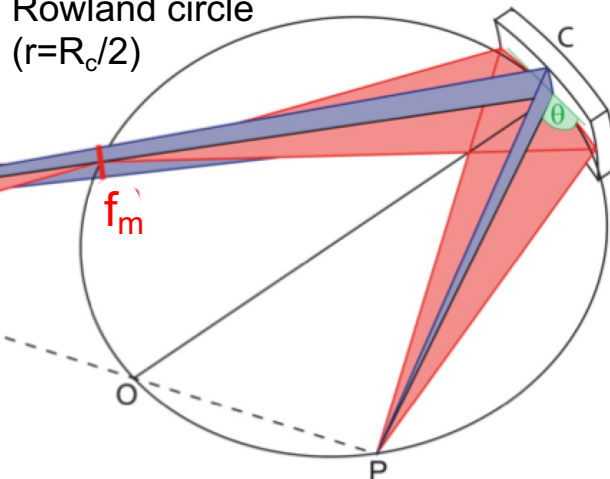


Typical distances from the crystal:

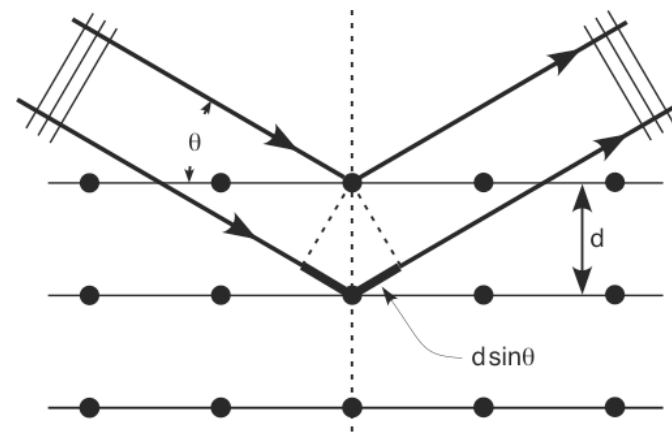
Meridional focus: $\Rightarrow f_m = R_c \sin \theta$

Sagittal focus: $\Rightarrow f_s = -f_m / \cos(2\theta)$

Rowland circle
($r=R_c/2$)



Crystals help achieving high-spectral response ($E/\Delta E > 10^4$) for high-resolution $T_{e,i}$ & $v_{\phi,\theta}$ measurements



① Bragg diffraction: $\Rightarrow 2d \sin \theta = n\lambda$

② Assuming a constant “d”, the observed relative wavelength shift (DS: Doppler shift) is given by:

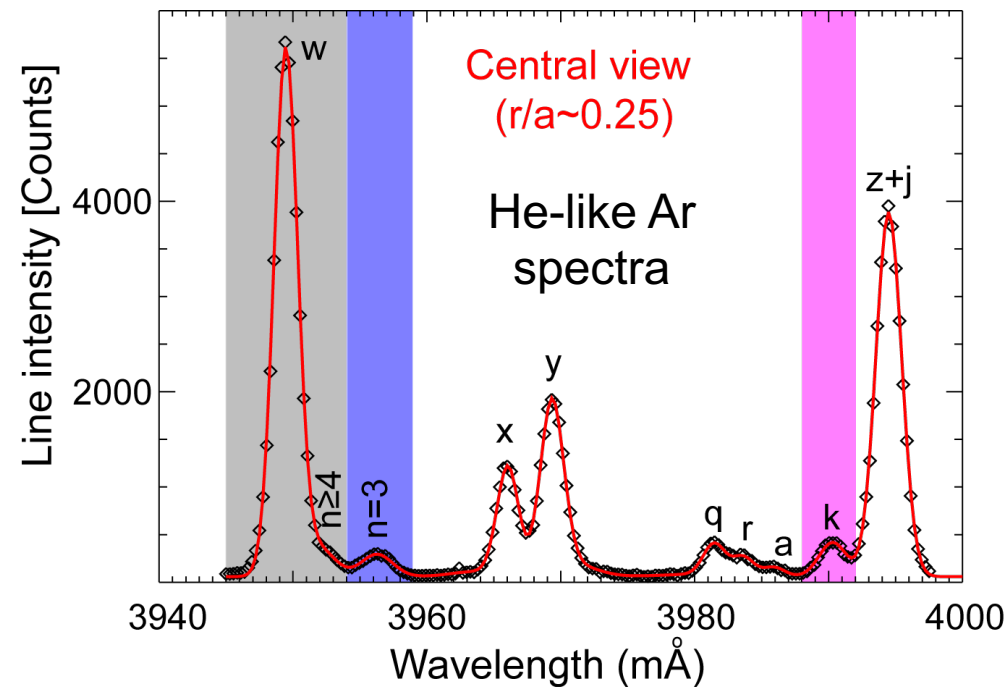
$$\Rightarrow \frac{\Delta\lambda}{\lambda_0} |_{DS} = \sqrt{\frac{1 + v/c}{1 - v/c}} \approx \frac{v}{c} \approx \frac{\Delta\theta}{\tan \theta}$$

v is the relative velocity between the source & detector

③ The value of $\Delta\theta_{\max}$ from Johann error (J_e): $(\Delta\theta)_{J_e} = l_c^2 / 8R_c^2 \tan \theta$

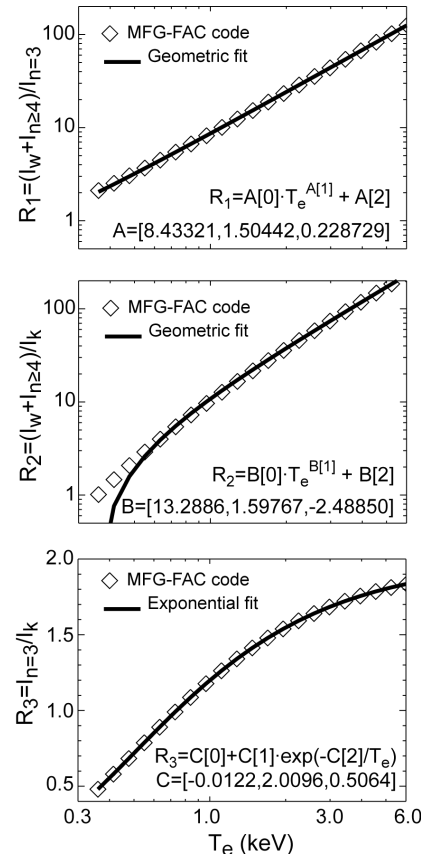
④ Resolving power: $\Rightarrow \frac{\lambda}{\Delta\lambda} = 8 \frac{R_c^2}{l_c^2} \tan^2 \theta$

Electron temperature T_e -profiles can also be obtained using line-ratios between resonance and satellite lines



T_e -measurements based on the ratio of the resonance line-w and the dielectronic satellites "n=3" and "k"

Considered to be a secondary diagnostic technique for the electron temperature (T_e) JT60SA and ITER.



(L. Delgado-Aparicio, unpublished)

Take home message: You have three alternatives (...but with multiple detection options) in the x-ray range !

① **Conventional broadband x-ray measurements**
(e.g. SXR tomography \Rightarrow confinement, MHD, equilibrium)

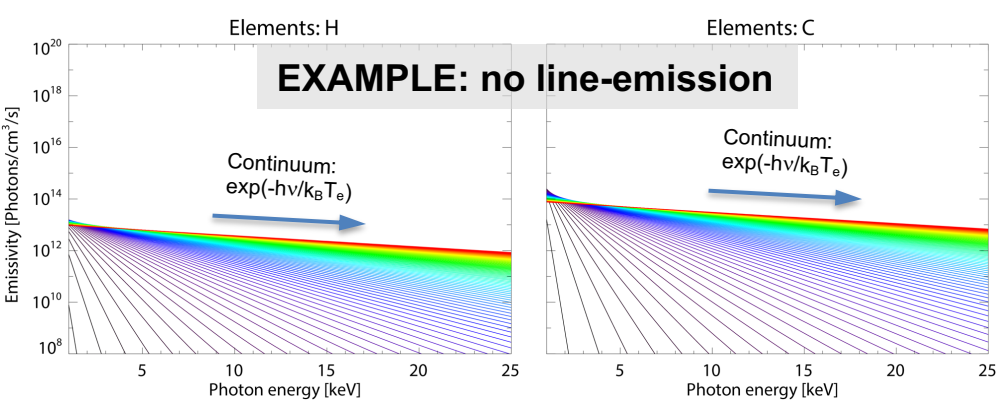
② **Doppler line-radiation x-ray measurements**
(e.g. n_Z , T_e , T_i , v_ϕ , v_θ , \Rightarrow calculation of E_r)

③ **Modern broadband PHA & multi-energy measurements**
(e.g. Z_{eff} , n_Z , T_e , $n_{e,\text{fast}}$)

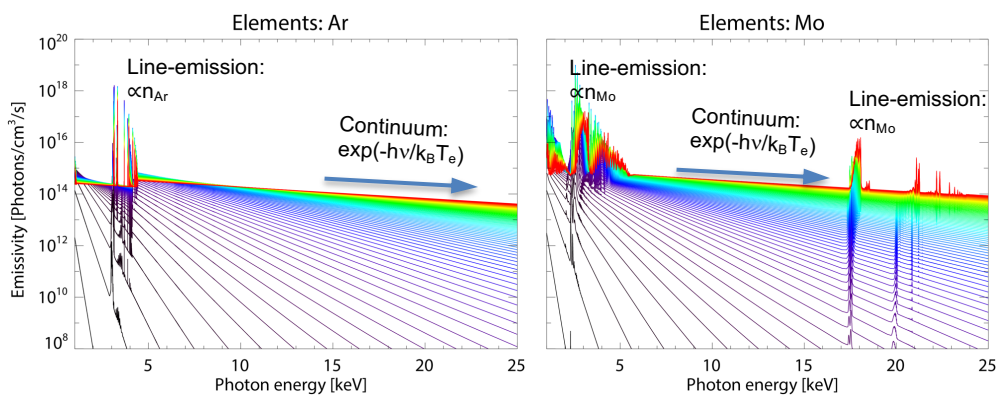
We also need to extract local plasma information !!!

Motivation #1: “spatially” resolve continuum & line-emission to derive local plasma physics parameters

EXAMPLE: no line-emission



?????



- Simultaneous:
- Time resolution
 - Spatial resolution
 - Energy resolution
 - In real-time...

Motivation #2: Develop ME-SXR imaging for magnetically confined fusion plasmas with a unique capability

Unique opportunity of measuring, *simultaneously*, a variety of plasma quantities:

a) electron temperature profiles ($T_e(R,t)$)

b) medium- to high-Z impurity

concentration profiles ($Z_{\text{eff}}, n_Z \Rightarrow \Delta Z_{\text{eff}}$)

c) the birth of suprathermal e⁻ ($n_{e,\text{fast}}$)

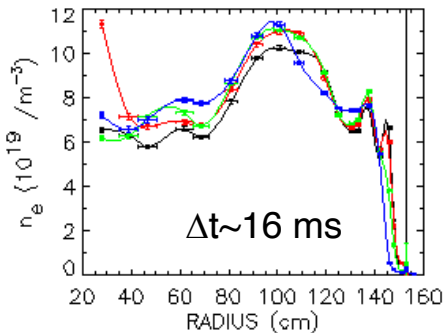
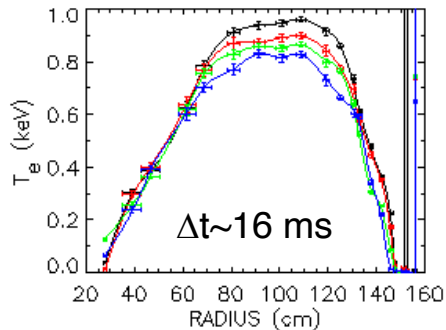
d) plasma position (R_0, Z_0)

Epecially applicable for:

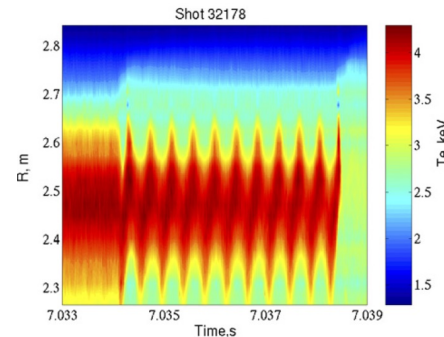
Spherical tokamaks: No T_e ECE-measurements in STs due to low- B_ϕ

Burning plasmas: Complement other techniques such as TS and ECE

NSTX's 60
Hz Multi-
point
Thomson
Scattering



Tore
Supra
fast ECE
data



Motivation #3: ... think really large (burning plasmas) !!!

Unique opportunity of measuring, *simultaneously*, a variety of plasma quantities:

a) electron temperature profiles ($T_e(R,t)$)

b) medium- to high-Z impurity

concentration profiles ($Z_{\text{eff}}, n_Z \Rightarrow \Delta Z_{\text{eff}}$)

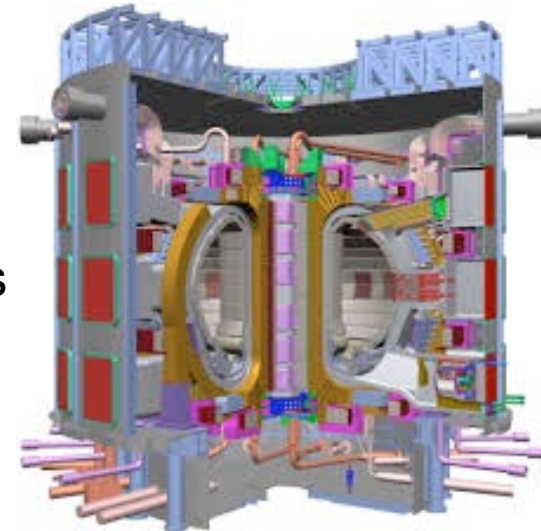
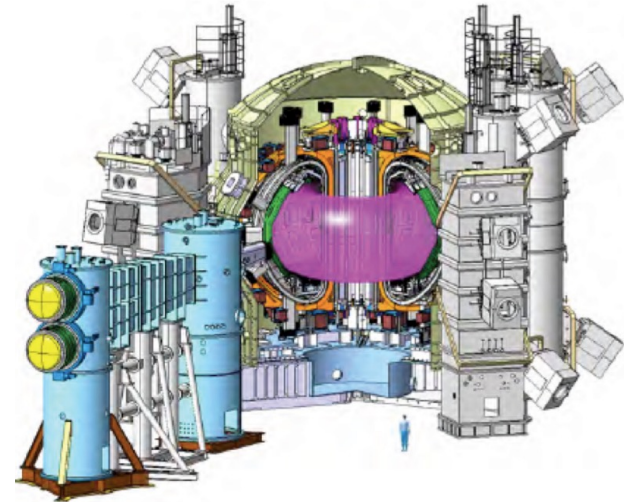
c) the birth of suprathermal e^- ($n_{e,\text{fast}}$)

d) plasma position (R_0, Z_0)

JT60SA, ITER & DEMO!

This technique should be explored also as a burning plasma diagnostic in-view of its simplicity and robustness.

e) $T_e(R,Z) \Rightarrow \Psi, J$ & q

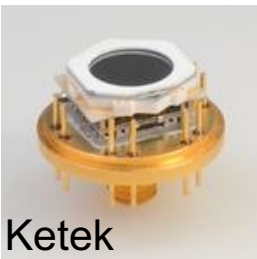


Background: Conventional photon counting ME-SXR systems use Si(Li), HgI₂, Si-Ge-CdTe diodes and SDDs

① Detectors in photon-counting mode

($\langle T_e \rangle$, $\langle Z_{\text{eff}} \rangle$, $\langle n_{e,\text{fast}} \rangle$, $\langle n_Z \rangle$)

- Pulse height analysis (PHA)
- Good energy resolution (100-200 eV)
- Slow time-response (20-50 ms)
- Low efficiency at high-energies
- Very poor profile definition
- Still used in our community (HT7, TCV, HL-2A)

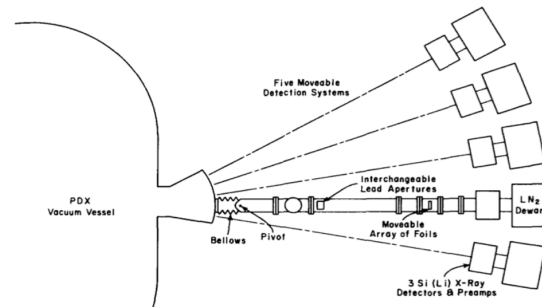
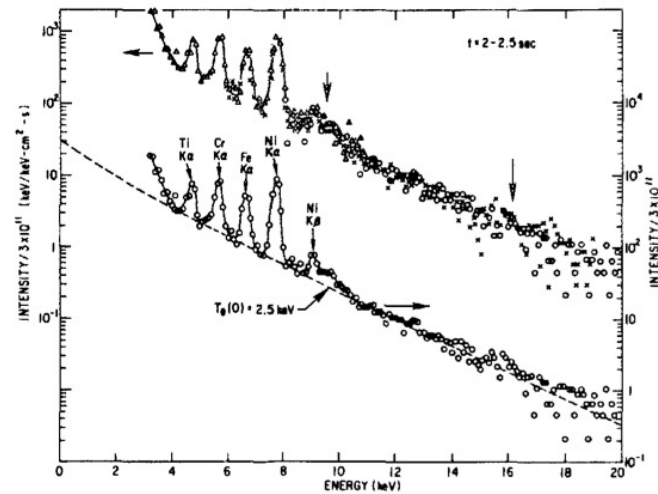


Ketek



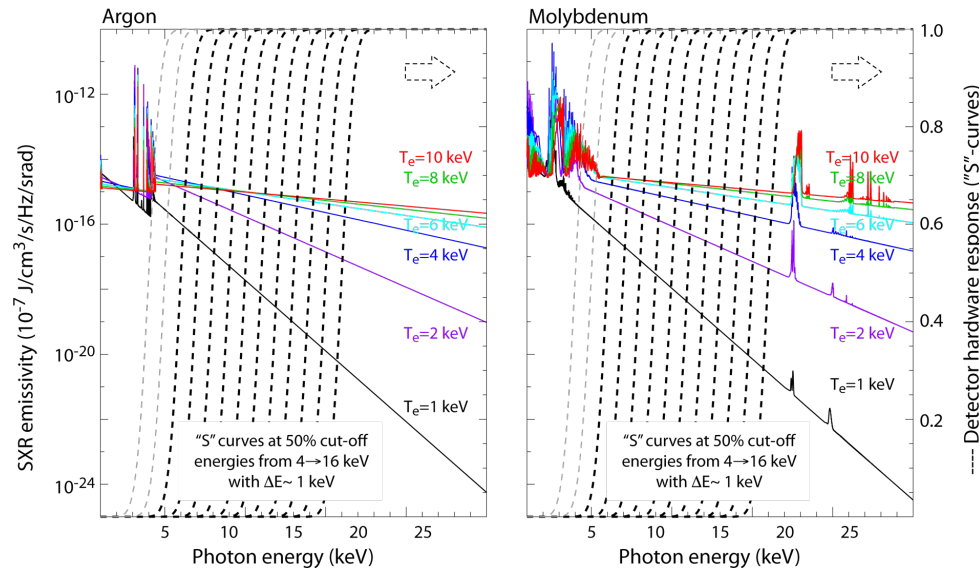
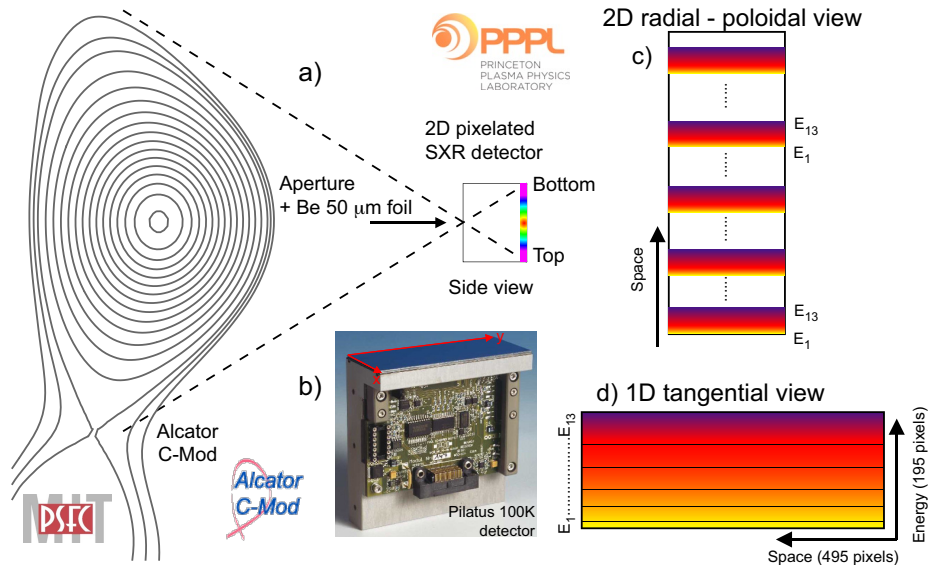
Amptek

Single-chord spectrometers



One spectrum per instrument

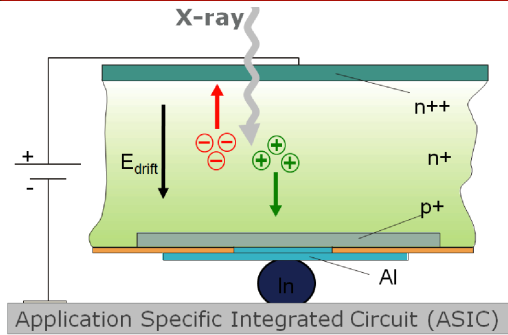
Initial ME-SXR imaging tests in C-Mod (@MIT) combined the best features from PHA & multi-foil methods



Pin-hole camera with multi-energy pixels allowed simultaneous spatial and energy resolution

From sampling the continuum radiation from Ar & Mo one can measure T_e & $n_e^2 Z_{\text{eff}}$

Pilatus silicon detectors enables breakthrough of 100k pixels (minimum) at single or multiple energy ranges



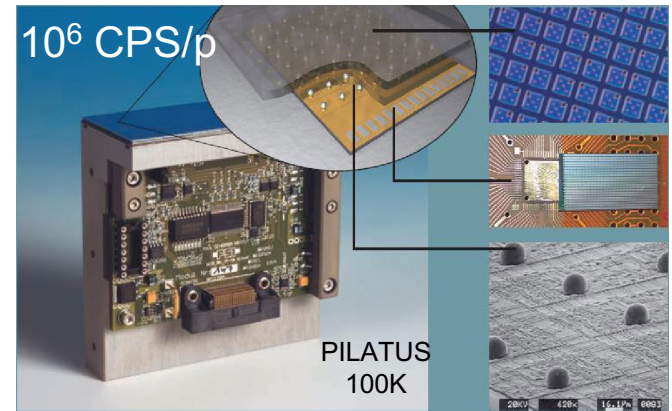
Operates in single photon counting mode

Thanks to important advances in the x-ray detector technology it is now possible to simultaneously record high resolution images of x-ray photons at single OR multiple energy ranges through direct x-ray detection.

CMOS hybrid pixel technology developed originally for synchrotrons (CERN + PSI + DECTRIS)



100K to 12M pixels (PILATUS: 172 μm , EIGER: 75 μm)

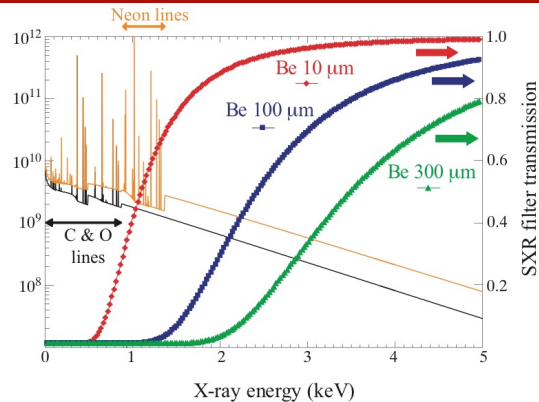


Si-sensor 2D array pn diodes
CMOS readout chip
In balls



PILATUS3 900K-IPP in-vacuum detector for x-ray plasma spectroscopy
(dimensions of a 100K system: 487x195 pixels)

Comparator and trimming voltages on each pixel allow individual coarse & fine tuning of energy range



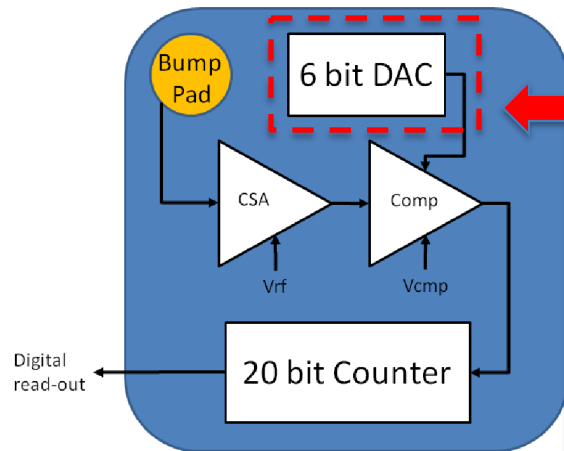
Filters: CXRO website:
X-ray database

$$\mathcal{T}(E) = \exp\left(-\frac{E_0^3}{E^3}\right)$$

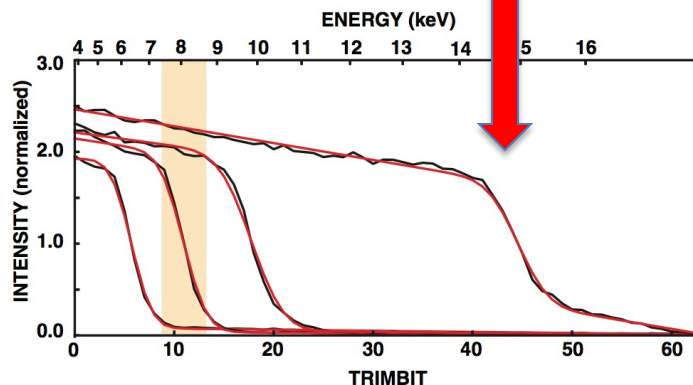
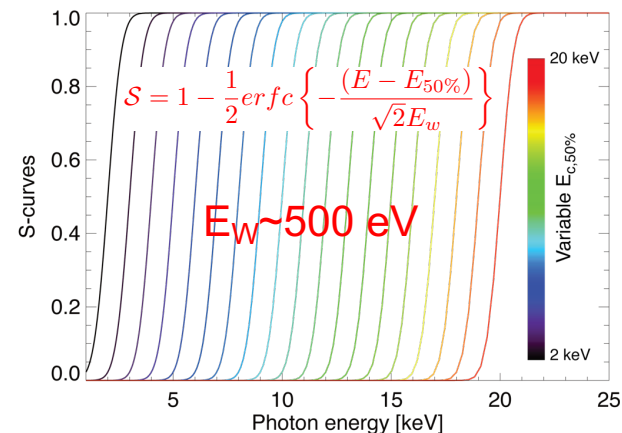
$$\Rightarrow \frac{d\mathcal{T}}{dE}\bigg|_{E_0} \sim \frac{1}{E_0}$$



“Constant” width of electronic response is a great improvement over the use of filters



PILATUS technology:
photon counting circuit in each pixel

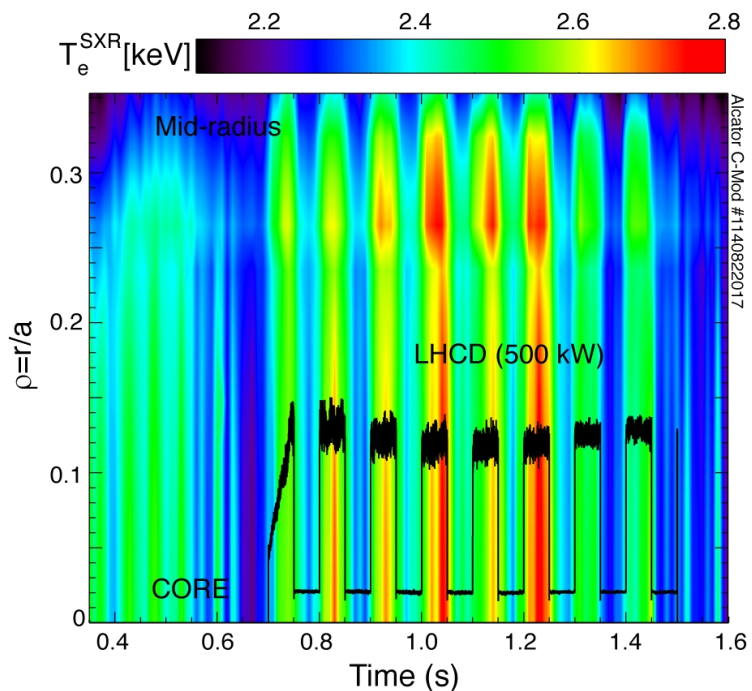
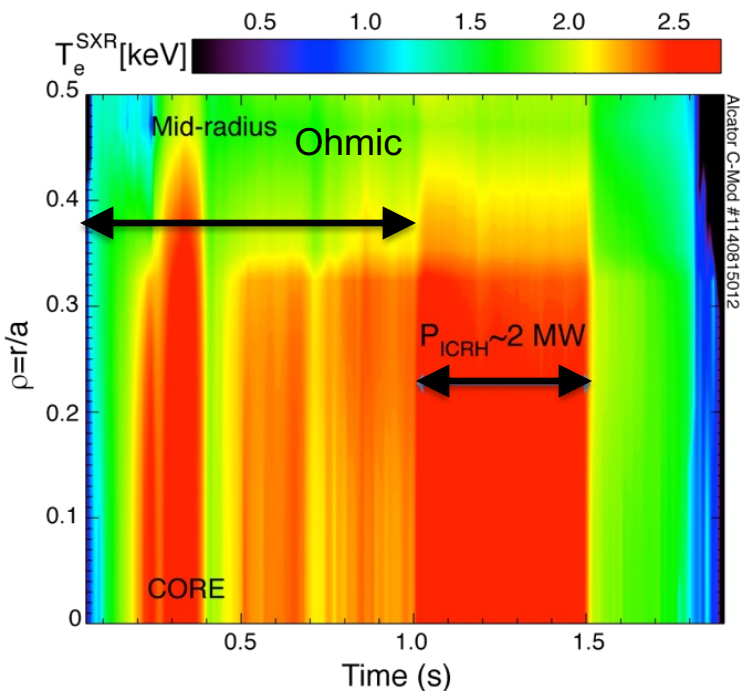


Goals #1&2: SXR-inferred T_e profiles can be obtained during Ohmic, ICRH & LHCD scenarios

- ICRH heats up ions & electrons
- EEDF function is still Maxwellian

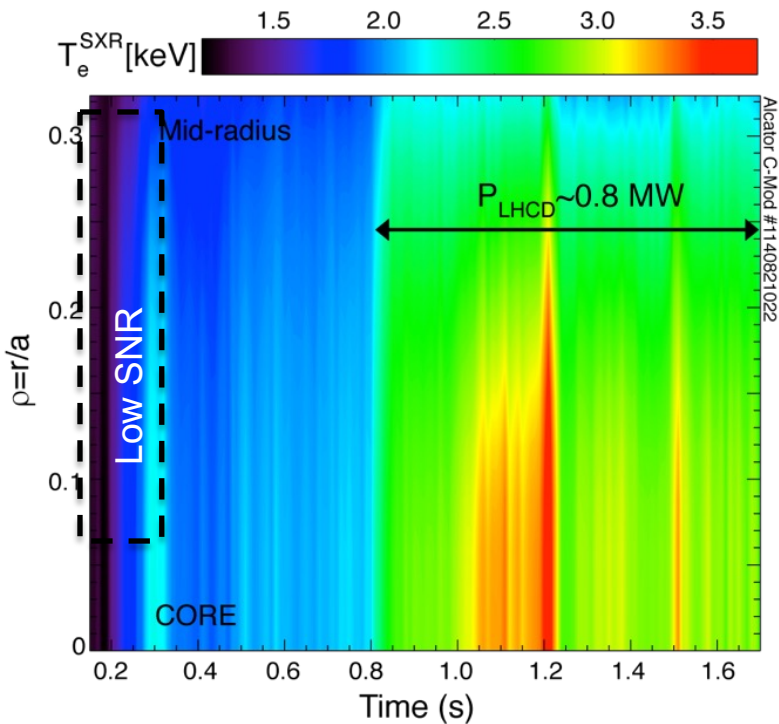
- LHCD drives current and heat e^-
- LHCD present challenges for ECE

Note:
Thin Si detectors are sensitive mostly to the Maxwellian part of the electron distribution function

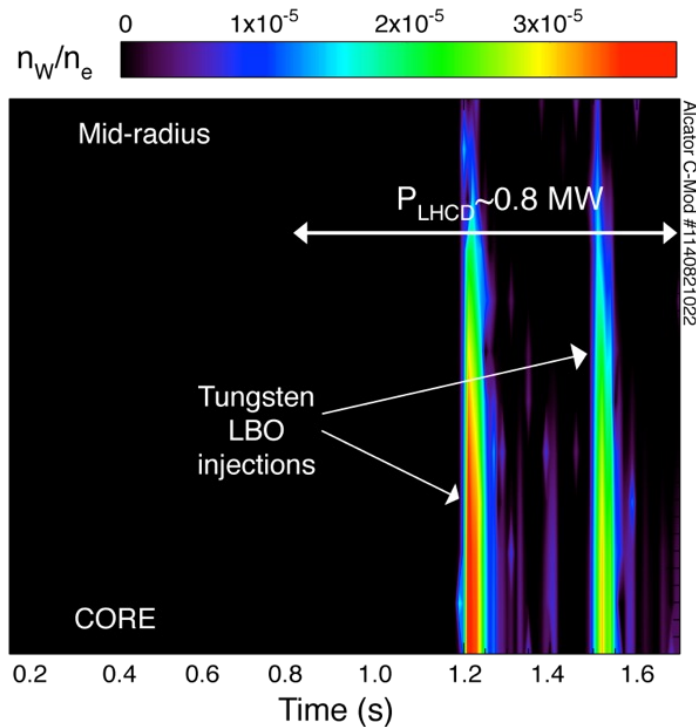


Goal #3: separate dynamic evolution of $T_e(R,t)$ from transient laser-blow-off contributions during LHCD

ME-SXR inferred $T_e(r,t)$



Tungsten density fraction

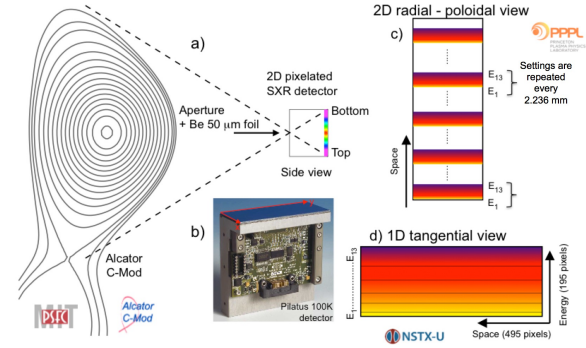
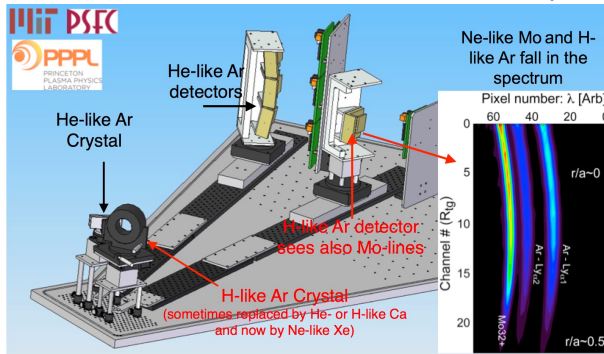
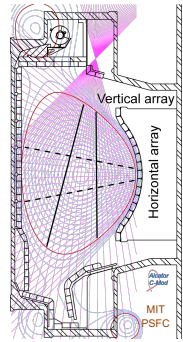


To-do:

- Estimate n_Z/n_e using other diagnostics and compare

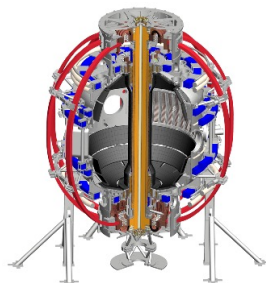
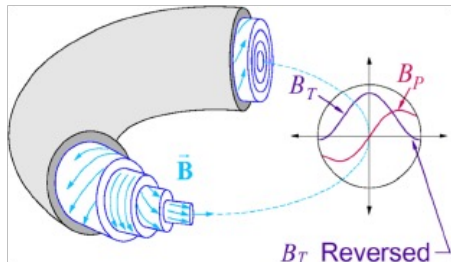
- Test Mo and W impurity transport in inductive & non-inductive scenarios

Summary: Modern x-ray diagnostics can help study MHD and resolve n_Z , $T_{e,i}$, $V_{\phi,\theta}$, Z_{eff} & $n_{e,\text{fast}}$ profiles



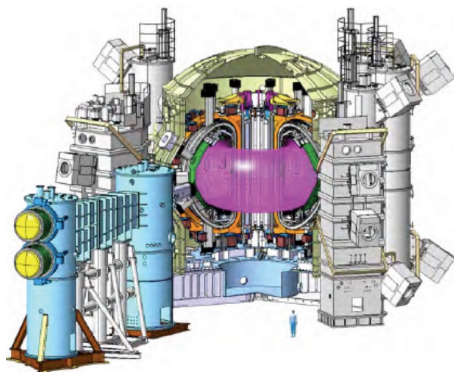
- ① With the selection of W for the divertor in ITER, understanding the sources, transport and confinement of high-Z impurities is crucial to ITER success.
- ② A significant fraction of the power delivered to the plasma is lost in the form of radiation. In the x-ray range (subset of P_{rad}) could be as high as 90%.
- ③ Modern diagnostics in x-ray range allow us to probe n_Z , $T_{e,i}$, $V_{\phi,\theta}$, Z_{eff} & $n_{e,\text{fast}}$ and their profiles!

New core x-ray diagnostic systems (US-lead) will be installed in NSTX-U, MST, WEST, JT60SA to ITER

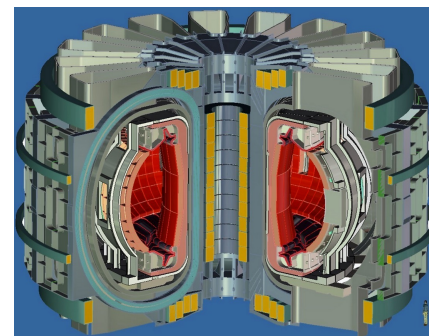
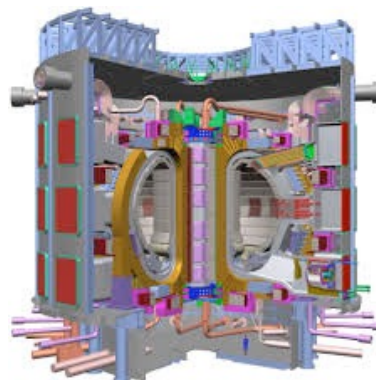


WEST - France

JT60SA
Japan



ITER
France



DEMO ?